

Special
Collection

Revealing the Heterogeneity of Large-Area MoS₂ Layers in the Electrocatalytic Hydrogen Evolution Reaction

Simon Schumacher,^[a] Lukas Madauß,^[b] Yossarian Liebsch,^[b] Emmanuel Batsa Tetteh,^[c] Swapnil Varhade,^[c] Wolfgang Schuhmann,^[c] Marika Schleberger,^[b] and Corina Andronescu*^[a]

The electrocatalytic activity concerning the hydrogen evolution reaction (HER) of micrometer-sized MoS₂ layers transferred on a glassy carbon surface was evaluated by scanning electrochemical cell microscopy (SECCM) in a high-throughput approach. Multiple areas on single or multiple MoS₂ layers were assessed using a hopping mode nanocapillary positioning with a hopping distance of 500 nm and a nanopipette size of around 55 nm. The locally recorded linear sweep voltammograms revealed a high lateral heterogeneity over the MoS₂ sheet

regarding their HER activity, with currents between –40 and –60 pA recorded at –0.89 V vs. reversible hydrogen electrode over about 4400 different measured areas on the MoS₂ sheet. Stacked MoS₂ layers did not show different electrocatalytic activity than the single MoS₂ sheet, suggesting that the interlayer resistance influences the electrocatalytic activity less than the resistances induced by possible polymer residues or water layers formed between the transferred MoS₂ sheet and the glassy carbon electrode.

Introduction

Two dimensional (2D) materials emerged in the last decades due to their unique properties, which open the way to new applications. Among those, transition metal dichalcogenides (TMDCs) were extensively studied for electrochemical applications, where they were used as electrocatalyst materials or to fabricate electrodes for different analyte detection.^[1] Inspired by nature, where hydrogenase enzymes contain Mo, Fe and Ni, nanosized MoS₂ was predicted by theory to be an efficient hydrogen evolution reaction (HER) electrocatalyst almost 20 years ago.^[2] Since then, many studies have confirmed the potential of MoS₂ as a highly active HER electrocatalyst.^[3–7]

Single MoS₂ layers show unique properties. They can be synthesised either in a bottom-up, e.g., chemical vapour deposition (CVD),^[8–10] or top-down, e.g., exfoliation, approach.^[11,12] While the latter generally offers high-quality 2D materials, it fails to produce large-scale single layers independ-

ently of the substrate and hence lacks scalability.^[10] Often, the transfer of MoS₂ layers on different supports is required, and recent studies indicate that this may also influence the properties of the MoS₂.^[13] Apart from the influence of the substrate itself, it was recently shown that intercalated water layers between the MoS₂ layers and the substrate substantially alter the MoS₂' electronic properties.^[14,15]

MoS₂ is seen as an abundant and lower-cost alternative for Pt as HER electrocatalyst.^[1,16] Improving the electrocatalytic activity of MoS₂ was attempted by different methods, such as doping with other elements,^[17,18] by introducing defects,^[4] or by applying strain.^[19] Multiple studies^[4,20–23] investigated the electrocatalytic activity of MoS₂ obtained via different synthesis routes at the macro- and nanoscale, leading to a debate about the location of active sites on MoS₂.^[24] While classical measurements performed at the macroscale can confirm an overall change in the electrocatalytic activity, they do not provide information about the active areas on the catalyst layer.


Scanning electrochemical cell microscopy (SECCM) demonstrated its power over the last decade in evaluating electrocatalyst materials at the nanoscale.^[25,26] In SECCM, a nanopipette filled with electrolyte is approached to the surface to be investigated. Upon contact, the hanging nano-droplet forms an electrochemical cell that allows the exclusive electrochemical evaluation of the wetted area. By automatically retracting and repositioning the nanopipette at different electrode areas, a high-throughput evaluation of the sample surface is achieved in a relatively short time.^[25] The technique is ideal for studying the lateral heterogeneity at the micro- and nanoscale and was used to evaluate electron-transfer rates or electrocatalytic activity of a broad range of materials such as Pt,^[27] carbon nanotubes,^[28] graphene,^[29–31] MoS₂,^[21,32,33] pentlandite crystals,^[34] Co(OH)₂ crystals,^[35] high-entropy alloys^[36] etc.


Initial studies at the nanoscale, reported by Bentley et al.,^[32] showed that the bulk MoS₂ basal plane possesses a high activity


[a] S. Schumacher, Prof. C. Andronescu
Chemical Technology III, Faculty of Chemistry and CENIDE; University of Duisburg-Essen
Carl-Benz-Straße 199, 47057 Duisburg, Germany
E-mail: corina.andronescu@uni-due.de

[b] Dr. L. Madauß, Y. Liebsch, Prof. M. Schleberger
Faculty of Physics and CENIDE; University of Duisburg-Essen
Duisburg, 47057, Germany

[c] E. B. Tetteh, S. Varhade, Prof. W. Schuhmann
Analytical Chemistry - Center for Electrochemical Sciences (CES), Faculty of Chemistry and Biochemistry
Ruhr University Bochum; Universitätsstraße 150, 44780 Bochum, Germany

 Supporting information for this article is available on the WWW under <https://doi.org/10.1002/celec.202200586>

 An invited contribution to the Early Career Women in Electrochemistry Special Collection

 © 2022 The Authors. ChemElectroChem published by Wiley-VCH GmbH. This is an open access article under the terms of the Creative Commons Attribution Non-Commercial NoDerivs License, which permits use and distribution in any medium, provided the original work is properly cited, the use is non-commercial and no modifications or adaptations are made.

towards HER, which significantly increases over the edge plane. The study of Takahashi et al. confirmed the existence of active sites on the basal space of small triangular MoS₂ layers having ~130 nm in length.^[21] They showed that on freshly prepared MoS₂, an increased activity could be observed for edges compared with the basal plane, a difference no longer visible when MoS₂ was exposed to air for several months.^[21] Cabre et al. evaluated the electron transfer rate for TMDCs exfoliated from bulk crystals on Au substrates.^[33] Plechinger et al. showed that CVD-grown MoS₂ could have a similar quality as exfoliated MoS₂ while having the advantage of larger and coherent single layers.^[37] These large single layers enable low-resolution and non-localised measurement methods, such as X-ray photoelectron spectroscopy (XPS), and open the door for the investigation of various structural modification methods, e.g., ion- or electron irradiation and etching. In catalytic and electrochemical applications, large reproducible single layers with a high surface coverage are desirable to maximise the surface-to-volume ratio.^[38]

In the present work, we evaluated the surface of large areas of single-sheet MoS₂ grown by CVD, which were transferred on a glassy carbon (GC) electrode using the classical polymer-assisted method. By probing 4941 different spots over an area of 30 μm × 40 μm (~4400 on the MoS₂ sheet), a variation of electrocatalytic HER activities was observed, and possible reasons for the increased lateral heterogeneity are discussed.

Results and Discussion

The single-layer MoS₂ sheet grown on a SiO₂/Si substrate, as previously reported,^[4] was transferred onto a GC electrode to enable mapping of the electrochemical activity of MoS₂ by SECCM. The GC electrode was used to establish the electrical connection (in the so-called bottom-contacted mode) and was further used as a working electrode (WE) in SECCM experiments. The mode of contacting the MoS₂ layers was shown to impact the measured electrocatalytic activity of MoS₂ by SECCM, since different pathways for the electrons transport are established. In top contact, the lateral electron transport along the layer occurs, while in bottom contact, the electron transfer occurs from the substrate to the upper MoS₂ sheet, where the reaction takes place. For example, in the case of bulk MoS₂, measuring with a top contact proved to be beneficial as compared to measuring with a bottom contact, as it prevented the recording linear sweep voltammograms (LSVs) with artefacts.^[32] On the other hand, for single to few-layer MoS₂, the bottom contact was successfully used to perform SECCM.^[33] For the large single-sheet MoS₂ used in this study, the recorded LSVs during the SECCM measurement show no artefacts (Figure S1), indicating that electrical conductivity between the MoS₂ sheet and the GC current collector is not limited.

SECCM measurements were performed with a capillary size of 55 nm in a hopping mode with a hopping step of 500 nm (Figure 1).

Based on the recorded LSVs, current maps are derived by plotting the currents recorded at defined potentials. At lower

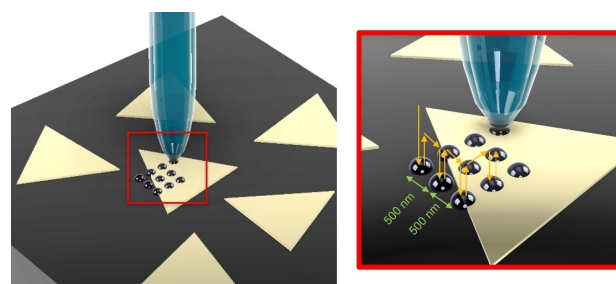


Figure 1. Schematic illustration of the SECCM hopping mode with a hopping distance of 500 nm.

overpotential [−0.6 V vs. reversible hydrogen electrode (RHE), Figure S2], slightly higher currents are recorded on the GC compared with the MoS₂ sheet.

At overpotentials lower than −0.6 V vs. RHE, we see a sudden increase in the currents recorded on the MoS₂ sheet compared to the GC (Figure 2, S2). Overall, over the MoS₂ sheet, we see a high variation of currents at −0.89 V vs. RHE, ranging from −20 to −60 pA (Figure S1), corresponding to current densities ranging from −0.45 to −1.36 A/cm² (Figure S3), in agreement with the results of Bentley et al.^[32] Exemplary LSVs from different locations are illustrated in Figure 2c. We compared the currents recorded on the GC at the beginning of the scan with those at the end of the scan to confirm the technical robustness of our experiment (white and black areas marked in Figure 2b). The histogram (Figure 2d) shows that on GC currents ranging between −7 and −24 pA are recorded, with an average of −15 ± 3 pA. Thus, we can confirm that no technical error occurred during the SECCM scan performed over 4941 landing sites, and the high current variation is caused by the MoS₂ structure only. Over the scan, lateral streaking can be observed over the scan direction, indicating changes in the droplet size. Such changes can be caused by differences in the surface's hydrophobicity/hydrophilicity due to residual polymers/water layers remaining on the MoS₂, after its transfer.

For example, in the region marked with pink in Figure 2b, the recorded currents at −0.89 V vs. RHE range between −20 to −40 pA, while in the red marked area higher currents between −40 to −60 pA are recorded. Locally, in an area of a few 1–2 μm², the MoS₂ sheet shows a relatively homogeneous catalytic activity, but significant differences are observed over extended ranges, as seen in Figure 2. SEM analysis of the transferred MoS₂ layers revealed the presence of regions where additional triangular-shaped MoS₂ layers with ~1 μm length are present on the MoS₂ single layers (Figure 2e and Figure 3a).

During the SECCM scan, several landings occurred on top of the multi-layer MoS₂ regions leading to LSVs recorded on a single or multiple MoS₂ layers. The footprint of the SECCM landing spot on the multilayered MoS₂ is marked by a red circle in the SEM image and the corresponding current with a red square in the resulting SECCM color map in Figure 3b. We do not observe significant differences between the single-layer or the multi-layer MoS₂ activities by comparing the recorded currents at the same potential. This indicates that the recorded

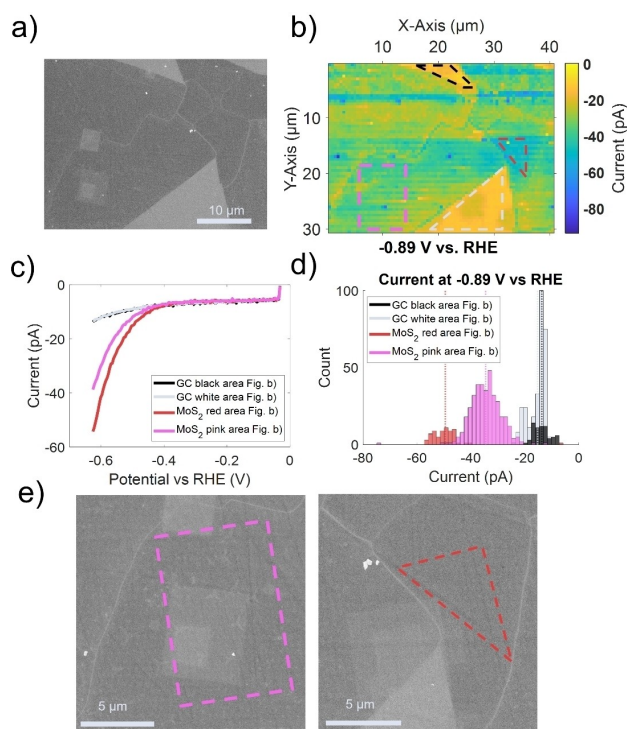


Figure 2. (a) Scanning electron microscopy (SEM) image of the MoS₂ sheet transferred on the GC on which the SECCM scan, containing 61 × 81 measured points, was performed. The SECCM scan spreads over an area of 40 μm × 30 μm with a hopping distance of 500 nm and a nanopipette tip size of ~55 nm. (b) Corresponding currents maps of the area marked in (a) derived by plotting the currents extracted from the recorded LSVs as a function of the measured position at -0.89 V vs. RHE. (c) Exemplary LSVs from different regions of the scan (GC top: X = 19.5 μm, Y = 1 μm; GC bottom: X = 29.5 μm, Y = 24 μm; MoS₂ high activity: X = 34 μm, Y = 15.5 μm; MoS₂ lower activity: X = 9.5 μm, Y = 23.5 μm). (d) Histograms showing the number of measured points for which different currents are recorded at -0.89 V vs. RHE in the areas marked with pink and red. The currents marked with white and black bars are currents recorded on the GC electrode. (e) SEM images of the areas marked with pink in which the presence of multiple MoS₂ layers (highlighted in Figure 3a) can be observed and SEM image of the area marked with red where no multi-layer MoS₂ can be identified.

catalytic activity on the transferred large area MoS₂ is stronger influenced by the electron transfer between the GC electrode and the first MoS₂ sheet. The results are in line with those reported by Takahashi et al. on small-sized MoS₂, where no difference was noticeable either in the HER electrocatalytic activity or the Tafel slope for single, two, or three layers of MoS₂.^[21] Based on the analysis of the areas containing single or multilayered MoS₂, we can conclude that the heterogeneity as observed in Figure 2 is not due to the presence of MoS₂ multi-layers. Polymer residues may still be present on top of the sample, equally affecting single and multi-layers. Another possible factor is the existence of a water layer/gas bubbles between the transferred MoS₂ and the GC surface, as we already reported previously.^[15] These intercalated water layers are commonly found in 2D samples exposed to ambient conditions. They occur in exfoliated samples as well, are difficult to remove and are known to affect the electronic properties.^[39–41]

Tafel analysis can provide information regarding the reaction mechanism and was extensively used to identify the rate-

limiting step in electrocatalytic driven processes.^[42] The Tafel slopes were automatically derived in the log(*i*)-range 2.5 to 3.5 and plotted similar to the activity maps (Figure 4a). To ensure a good quality of the data fitting used to derive the Tafel plots, we checked the value of the coefficient of determination (*R*²) automatically calculated for each measured plot (Figure 4b). *R*² values ranging from 0.9–1 were obtained for most of the points (~95%). The points with values outside this range were removed (white points in Figures 4a, 4b).

The distribution of calculated Tafel slopes over the SECCM scan is presented as a histogram in Figure S4, where Tafel slopes with values ranging between 80–120 mV/dec for the majority of measured points. These values indicate the Volmer step or, according to predicted models, the Heyrovsky step at high coverages rates as the rate-determining step.^[42] For a limited number of points (mainly located on the GC surface), we obtained higher values of the Tafel slopes than those theoretically expected. Overall, the recorded Tafel plots support the HER activity of the basal planes. They agree with several other reports, which show that the basal planes of pristine MoS₂ are present on the MoS₂ single layers (Figure 2e and Figure 3a) and are not highly electrocatalytically active but similar to the ones of Au and Cu.^[32]

Conclusion

The lateral heterogeneity of large single layers of MoS₂ grown by CVD and subsequently transferred to a GC was evaluated by SECCM in a hopping mode using a nm-sized nanopipette. The activity maps revealed a high lateral heterogeneity which becomes significant over longer ranges. Since no difference in activity was recorded for single and multi-layer MoS₂, we attribute the observed lateral heterogeneity to the presence of polymer residues or the presence of a water layer/gas bubbles between the MoS₂ sheet and the GC formed during the transfer process. The Tafel slopes and the recorded current densities indicate a moderate HER activity of the large-area MoS₂ transferred on the GC, similar to that of the exfoliated MoS₂ layers reported in literature.

Experimental Section

Synthesis of Large-Scale MoS₂ and Transfer on the GC

Large-scale single-layer MoS₂ was synthesised in a custom CVD process. The precursor, a droplet of ammonium heptamolybdate (AHM) solution, was placed on a piece of silicon with a 300 nm thick oxide layer. Subsequently, the sample was dried at 300 °C for 24 min, and a seeding promotor (1% sodium cholate acid solution dissolved in H₂O) was applied using a spin-coater. Each precursor, sulfur being the second, is placed into a separate crucible and is positioned in a furnace with different heating zones. The sulfur crucible is placed into the first heating zone, while the crucible with the silicon piece is placed downstream into the second heating zone. An optimised heating profile makes sure that each precursor enters the gas phase simultaneously. During the process, argon flows through the quartz tube to suppress chemical reactions with

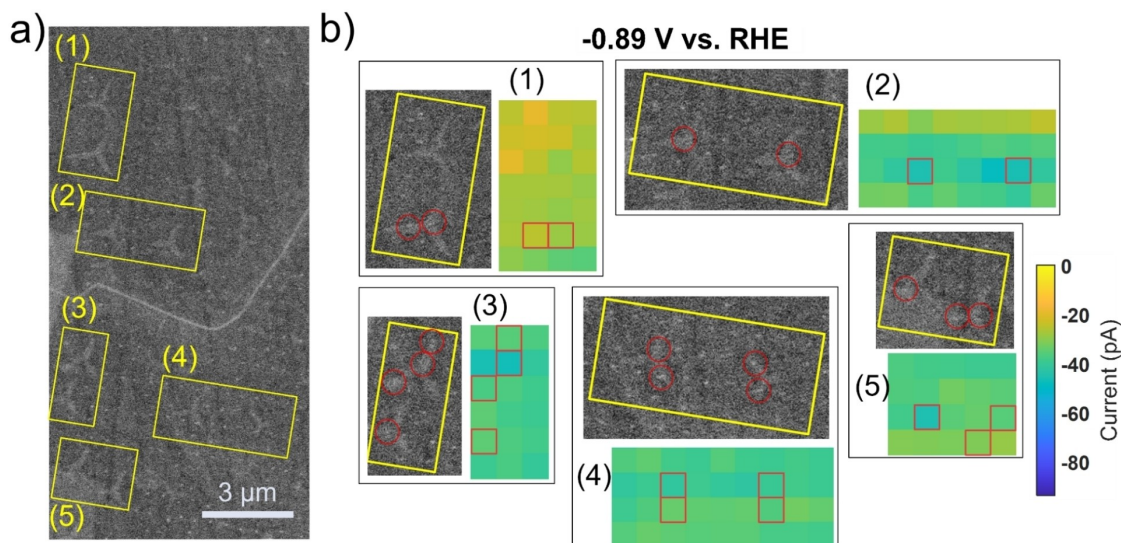


Figure 3. (a) SEM image of the MoS₂ sheet transferred on the GC after performing the SECCM experiment on which one can observe the areas in contact with the electrolyte droplet as well as the additional MoS₂ layers present on the large-area MoS₂, which are marked for a better identification; (b) the SEM areas and the corresponding activity maps derived by plotting the currents recorded at -0.89 V vs. RHE as a function of the measured pixel for the marked regions in which single or multilayered MoS₂ are evaluated in the SECCM experiment.

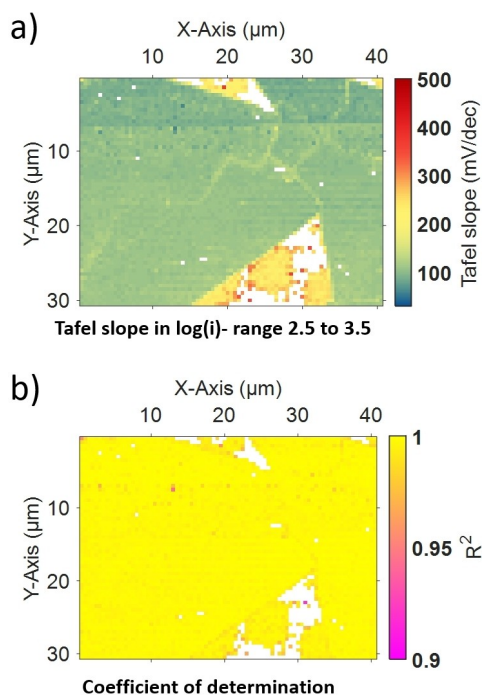


Figure 4. Tafel plot analysis of the SECCM scan presented in Figures 2 and S1. (a) Tafel slopes and (b) their corresponding coefficient of determination (R^2) as a function of the position in the SECCM scan.

air, e.g., oxidation. After 30 min, the samples can be retrieved. To transfer the grown MoS₂ flakes onto the glassy carbon substrate, poly(methyl methacrylate) (PMMA) was spin-coated onto the samples. Then, the sample was placed into a 0.1 M KOH bath, slowly etching the SiO₂ and separating the PMMA/MoS₂ layer from the silicon piece. After that, the resulting layer of PMMA/MoS₂ was transferred into a water bath to clean it, and it could then be scooped off with the glassy carbon substrate. The glassy carbon was purchased (HTW Hochttemperatur-Werkstoffe GmbH) in a

polished condition. The roughness of the glassy carbon surface was measured in an atomic force microscope (AFM) to 2.5 ± 0.5 nm. In the last step, acetone was applied to the PMMA/MoS₂ layer to dissolve the remaining PMMA.

Scanning Electrochemical Cell Microscopy

Single barrel pipettes with nanometer-sized tip openings were fabricated by laser pulling single barrel quartz glass capillaries using a CO₂-laser puller (P-2000; Sutter Instruments). A one-line program with the following pulling parameters was used: HEAT 790, FIL 4, VEL 40, DEL 130, PUL 110, generating a nanopipette with an opening diameter of approximately 55 nm (Figure S5). The obtained nanopipettes were filled with 0.1 M HClO₄ using a MicroFil syringe, and a Ag/AgCl wire was inserted and used as quasi reference counter electrode (QRCE) during the SECCM experiments. To fabricate the Ag/AgCl QRCE, a polished Ag wire (diameter: 0.125 mm, Goodfellow, 99,99%) was immersed in a 3 M KCl + 0.1 M HCl solution, and a potential of +5 V versus a Pt electrode was applied for 10 min. The QRCE open circuit potential was measured vs a Ag|AgCl|3 M KCl reference electrode before and after the SECCM measurement. The filled nanopipette and the Ag/AgCl/3 M KCl were immersed in a one-compartment cell filled with 0.1 M HClO₄ and the open circuit potential (E_{OCP}) was measured with a digital potentiometer. The conversion of the potentials applied during the SECCM measurements vs. the Ag/AgCl QRCE to the RHE scale was performed using the following equation:

$$E_{\text{RHE}} [\text{V}] = E_{\text{Ag/AgCl}} + 0.210 + E_{\text{OCP}} + 0.059 \text{ pH},$$

where $E_{\text{Ag/AgCl}}$ is the applied potential to the working electrode versus the QRCE, 0.210 V is the standard potential of the Ag|AgCl|3 M KCl reference electrode, and E_{OCP} is the correction factor of the open circuit potential measured against the commercial reference electrode (31 mV). 0.059 is the result of $(RT) \cdot (nF)^{-1}$, with R the universal gas constant, T the temperature ($25^\circ\text{C} = 298^\circ\text{K}$), F the Faraday constant and n equals 1.

Electrochemical measurements were performed in a home-built SECCM workstation.^[43] A sample holder supporting the GC/MoS₂ sample is mounted on a 3-axis step motor microscrew system (Owis) and controlled by an L-Step PCIe controller card (Lang). This enables a coarse positioning and first approach of the pipette tip to approximately 50 μm above the surface.

The filled single barrel capillary with the QRCE is mounted at a 3-axis piezo nanopositioner (P-611.3S nanocube, Physik Instrumente). For fine positioning of the pipette tip above the surface, an analog amplifier (E-664, Physik Instrumente) is used.

In the electrochemical experiments, the MoS₂ sample transferred on the GC is used as WE and the Ag/AgCl-wire as QRCE in a 2-electrode system. The electrochemical cell is established after approaching the MoS₂/GC sample towards the nanopipette having a hanging drop. Once the MoS₂/GC makes contact with the hanging drop, an electrochemical cell is formed. The surface contact is detected by measuring the current between the WE and the QRCE, stopping the approach immediately after a current threshold of -2 pA is recorded using a low noise current amplifier (DLPCA-200, FEMTO). The size of the formed electrochemical cell depends on the capillary opening which is estimated based on the size of the nanopipette opening.

Using a hopping-mode measurement protocol a spatial resolution was possible by measuring 61 × 81 individual spots with a distance of 500 nm, resulting in a map of 30 × 40 μm.

Scanning Electron Microscopy

For the characterisation of the nanopipette tip (size measurement of the opening) and the analysis of the landing spots during the SECCM scan, a Quanta 3D ESEM (FEI) microscope was used.

Acknowledgements

S.S., C.A. acknowledge financial support from the German Research Foundation (Deutsche Forschungsgemeinschaft, DFG) in the framework of the DFG project AN 1570/2-1 (440951282). L.M., Y.L. and M.S. acknowledge support from the German Research Foundation (DFG) under project SCHL 384/20-1 (406129719). W.S. and E.B.T received funding from the European Research Council (ERC) under the European Union's Horizon 2020 research and innovation program (grant agreement CasCat [833408]) as well as under the Marie Skłodowska-Curie MSCA-ITN, Sentinel [812398]. Prof. Patrick Unwin from the University of Warwick is acknowledged for providing the initial SECCM control software (WEC-SPM). Open Access funding enabled and organized by Projekt DEAL.

Conflict of Interest

The authors declare no conflict of interest.

Data Availability Statement

The data that support the findings of this study are available from the corresponding author upon reasonable request.

Keywords: chemical vapour deposition · hydrogen evolution reaction · molybdenum disulfide · scanning electrochemical cell microscopy · thin film materials

- [1] X. Chia, A. Y. S. Eng, A. Ambrosi, S. M. Tan, M. Pumera, *Chem. Rev.* **2015**, *115*, 11941.
- [2] B. Hinnemann, P. G. Moses, J. Bonde, K. P. Jørgensen, J. H. Nielsen, S. Horch, I. Chorkendorff, J. K. Nørskov, *J. Am. Chem. Soc.* **2005**, *127*, 5308.
- [3] Z. Cui, W. Du, C. Xiao, Q. Li, R. Sa, C. Sun, Z. Ma, *Front. Phys.* **2020**, *15*, 63502.
- [4] L. Madauß, I. Zegkinoglou, H. Vázquez Muiños, Y.-W. Choi, S. Kunze, M.-Q. Zhao, C. H. Naylor, P. Ernst, E. Pollmann, O. Ochedowski, H. Lebius, A. Benyagoub, B. Ban-d'Etat, A. T. C. Johnson, F. Djurabekova, B. Roland Cuenya, M. Schleberger, *Nanoscale* **2018**, *10*, 22908.
- [5] S. Niu, J. Cai, G. Wang, *Nano Res.* **2021**, *14*, 1985.
- [6] T. F. Jaramillo, K. P. Jørgensen, J. Bonde, J. H. Nielsen, S. Horch, I. Chorkendorff, *Science* **2007**, *317*, 100.
- [7] J. Kibsgaard, Z. Chen, B. N. Reinecke, T. F. Jaramillo, *Nat. Mater.* **2012**, *11*, 963.
- [8] E. Pollmann, J. M. Morbec, L. Madauß, L. Bröckers, P. Kratzer, M. Schleberger, *J. Phys. Chem. C* **2020**, *124*, 2689.
- [9] J. Sitek, J. Plocharski, I. Pasternak, A. P. Gertych, C. McAleese, B. R. Conran, M. Zdrojek, W. Strupinski, *ACS Appl. Mater. Interfaces* **2020**, *12*, 45101.
- [10] S. H. Baek, Y. Choi, W. Choi, *Nanoscale Res. Lett.* **2015**, *10*, 388.
- [11] E. Pollmann, S. Sleziona, T. Foller, U. Hagemann, C. Gorynski, O. Petri, L. Madauß, L. Breuer, M. Schleberger, *ACS Omega* **2021**, *6*, 15929.
- [12] F. Liu, *Prog. Surf. Sci.* **2021**, *96*, 100626.
- [13] M. Buscema, G. A. Steele, H. S. J. van der Zant, A. Castellanos-Gomez, *Nano Res.* **2014**, *7*, 561.
- [14] J. O. Varghese, P. Agbo, A. M. Sutherland, V. W. Brar, G. R. Rossman, H. B. Gray, J. R. Heath, *Adv. Mater.* **2015**, *27*, 2734.
- [15] E. Pollmann, L. Madauß, S. Schumacher, U. Kumar, F. Heuvel, C. vom Ende, S. Yilmaz, S. Güngörmüs, M. Schleberger, *Nanotechnology* **2020**, *31*, 505604.
- [16] J. Bonde, P. G. Moses, T. F. Jaramillo, J. K. Nørskov, I. Chorkendorff, *Faraday Discuss.* **2008**, *140*, 219–231.
- [17] J. Xu, Z. Zhao, W. Wei, G. Chang, Z. Xie, W. Guo, D. Liu, D. Qu, H. Tang, J. Li, *Chemistry* **2021**, *27*, 15992.
- [18] T. H. M. Lau, X. Lu, J. Kulhavy, S. Wu, L. Lu, T.-S. Wu, R. Kato, J. S. Foord, Y.-L. Soo, K. Suenaga, S. C. E. Tsang, *Chem. Sci.* **2018**, *9*, 4769.
- [19] Y. Da Hwang, K. H. Choi, J. E. Park, D. H. Suh, *Phys. Chem. Chem. Phys.* **2017**, *19*, 18356.
- [20] U. Krishnan, M. Kaur, K. Singh, M. Kumar, A. Kumar, *Superlattices Microstruct.* **2019**, *128*, 274.
- [21] Y. Takahashi, Y. Kobayashi, Z. Wang, Y. Ito, M. Ota, H. Ida, A. Kumatani, K. Miyazawa, T. Fujita, H. Shiku, Y. E. Korchev, Y. Miyata, T. Fukuma, M. Chen, T. Matsue, *Angew. Chem. Int. Ed.* **2020**, *59*, 3601.
- [22] G. Ye, Y. Gong, J. Lin, B. Li, Y. He, S. T. Pantelides, W. Zhou, R. Vajtai, P. M. Ajayan, *Nano Lett.* **2016**, *16*, 1097.
- [23] L. Tao, X. Duan, C. Wang, X. Duan, S. Wang, *Chem. Commun.* **2015**, *51*, 7470.
- [24] J. Zhang, J. Wu, H. Guo, W. Chen, J. Yuan, U. Martinez, G. Gupta, A. Mohite, P. M. Ajayan, J. Lou, *Adv. Mater.* **2017**, *29*, 1701955.
- [25] C. L. Bentley, M. Kang, P. R. Unwin, *J. Am. Chem. Soc.* **2017**, *139*, 16813.
- [26] C. L. Bentley, J. Edmondson, G. N. Meloni, D. Pery, V. Shkirskiy, P. R. Unwin, *Anal. Chem.* **2019**, *91*, 84.
- [27] B. D. B. Aaronson, C.-H. Chen, H. Li, M. T. M. Koper, S. C. S. Lai, P. R. Unwin, *J. Am. Chem. Soc.* **2013**, *135*, 3873.
- [28] A. G. Güell, N. Ebejer, M. E. Snowden, K. McKelvey, J. V. Macpherson, P. R. Unwin, *Proc. Natl. Acad. Sci. USA* **2012**, *109*, 11487.
- [29] G. Zhang, P. M. Kirkman, A. N. Patel, A. S. Cuharuc, K. McKelvey, P. R. Unwin, *J. Am. Chem. Soc.* **2014**, *136*, 11444.
- [30] A. G. Güell, A. S. Cuharuc, Y.-R. Kim, G. Zhang, S. Tan, N. Ebejer, P. R. Unwin, *ACS Nano* **2015**, *9*, 3558.
- [31] A. G. Güell, N. Ebejer, M. E. Snowden, J. V. Macpherson, P. R. Unwin, *J. Am. Chem. Soc.* **2012**, *134*, 7258.
- [32] C. L. Bentley, M. Kang, F. M. Maddar, F. Li, M. Walker, J. Zhang, P. R. Unwin, *Chem. Sci.* **2017**, *8*, 6583.
- [33] M. Brunet Cabré, A. E. Paiva, M. Velický, P. E. Colavita, K. McKelvey, *Electrochim. Acta* **2021**, *393*, 139027.

- [34] C. L. Bentley, C. Andronescu, M. Smialkowski, M. Kang, T. Tarnev, B. Marler, P. R. Unwin, U.-P. Apfel, W. Schuhmann, *Angew. Chem. Int. Ed.* **2018**, *57*, 4093.
- [35] J. T. Mefford, A. R. Akbashev, M. Kang, C. L. Bentley, W. E. Gent, H. D. Deng, D. H. Alsem, Y.-S. Yu, N. J. Salmon, D. A. Shapiro, P. R. Unwin, W. C. Chueh, *Nature* **2021**, *593*, 67.
- [36] E. B. Tetteh, L. Banko, O. A. Krysiak, T. Löffler, B. Xiao, S. Varhade, S. Schumacher, A. Savan, C. Andronescu, A. Ludwig, W. Schuhmann, *Electrochem. Sci. Adv.* **2021**, *2*, e2100105.
- [37] G. Plechinger, J. Mann, E. Preciado, D. Barroso, A. Nguyen, J. Eroms, C. Schüller, L. Bartels, T. Korn, *Semicond. Sci. Technol.* **2014**, *29*, 64008.
- [38] D. F. van der Vliet, C. Wang, D. Tripkovic, D. Strmcnik, X. F. Zhang, M. K. Debe, R. T. Atanasoski, N. M. Markovic, V. R. Stamenkovic, *Nat. Mater.* **2012**, *11*, 1051.
- [39] O. Ochedowski, B. K. Bussmann, M. Schleberger, *Sci. Rep.* **2014**, *4*, 6003.
- [40] M. Temmen, O. Ochedowski, M. Schleberger, M. Reichling, T. R. J. Bollmann, *New J. Phys.* **2014**, *16*, 53039.
- [41] O. Ochedowski, K. Marinov, N. Scheuschner, A. Poloczek, B. K. Bussmann, J. Maultzsch, M. Schleberger, *Beilstein J. Nanotechnol.* **2014**, *5*, 291.
- [42] T. Shinagawa, A. T. Garcia-Esparza, K. Takanabe, *Sci. Rep.* **2015**, *5*, 13801.
- [43] T. Tarnev, H. B. Aiyappa, A. Botz, T. Erichsen, A. Ernst, C. Andronescu, W. Schuhmann, *Angew. Chem. Int. Ed.* **2019**, *58*, 14265.

Manuscript received: May 24, 2022

Revised manuscript received: June 27, 2022

Accepted manuscript online: August 2, 2022